


Generation of Non-Rayleigh Nondiffracting Speckles

Ruifeng Liu^{1,*}, Bingcheng Qing^{1,*}, Shupeng Zhao¹, Pei Zhang¹, Hong Gao¹, Shouqian Chen^{2,†} and Fuli Li^{1,‡}

¹*Shaanxi Province Key Laboratory of Quantum Information and Quantum Optoelectronic Devices, School of Physics, Xi'an Jiaotong University, Xi'an 710049, People's Republic of China*

²*Research Center for Space Optics Engineering, Harbin Institute of Technology, Heilongjiang, Harbin 150001, People's Republic of China*

 (Received 7 December 2020; accepted 29 September 2021; published 26 October 2021)

Optical speckle fields with both non-Rayleigh statistics and nondiffracting characteristics in propagation are an important light source for many applications. However, tailoring either non-Rayleigh statistical speckles or nondiffracting speckles are only investigated independently in previous studies. Here, we report the first observation of optical speckles that remain diffraction-free over a long axial distance while keeping non-Rayleigh statistics simultaneously. We further show the enhancement of Anderson localization of light with the non-Rayleigh nondiffracting speckles. The work presented here provides a versatile framework for customizing optical fields with desired speckle patterns for applications in the fields of solid-state physics, cold atoms, and optical imaging.

DOI: [10.1103/PhysRevLett.127.180601](https://doi.org/10.1103/PhysRevLett.127.180601)

Speckles appear when a coherent wave transmits through a complex medium or is reflected from a rough surface. The statistical property of a speckle pattern is generally universal and commonly referred to as Rayleigh statistics featuring a negative-exponential intensity probability density function (PDF) [1]. The reason why speckles typically exhibit Rayleigh statistics is that the field results from the interference of a large number of independent partial waves with random phases uniformly distributed over a range of 2π . However, non-Rayleigh statistical speckles are valuable resources for many applications such as ghost imaging [2–4], structured illumination microscopy [5–8], and fundamental research [9]. Various schemes have been proposed to generate non-Rayleigh statistical speckles [10–18]. By tailoring the higher-order correlations of the scattered partial waves, super-Rayleigh and sub-Rayleigh speckles can be generated on a target plane [11]. Speckle patterns with arbitrarily tailored intensity PDF can also be generated by judiciously modulating the wavefront of a monochromatic laser beam [17].

An optical field initially confined to a finite area in a transverse plane will be subject to diffractive spreading as propagating outward from that plane in a free space. So, the intensity profile of speckles changes as the beam propagates, and keeps stable only in the Rayleigh range corresponding to the transverse length of a single speckle [19,20]. Although the non-Rayleigh statistics can be introduced on a certain plane [10–18], the intensity profile of the speckles will change and generally lose the non-Rayleigh statistics while propagating.

In 1987, Durnin *et al.* found the exact solutions of the scalar wave equation for nondiffracting beams [21]. One of the best-known examples is the zero-order Bessel beam,

which can be generated by illuminating a ring-shaped slit located in the focal plane of a lens [22]. The work paved a way toward the discovery of other interesting nondiffracting optical fields [23–26] and sparked considerable studies for volumetric imaging [27], nondiffracting pulsed beams [28,29], and particle manipulation [30]. Turunen *et al.* first introduced the field of random nondiffracting speckles [31]. They showed that nondiffracting speckles can be generated by introducing random phases independently distributed over 0 to 2π on the Durnin's ring-shaped slit [22]. Since then, several modified schemes are proposed to generate nondiffracting speckles with computer-generated holograms [32–35] and degenerate cavity laser [36]. Since an optical field with nondiffracting speckles has an infinite depth of field (DOF) in theory, it can be used to increase the local DOF of a computational ghost imaging system [37]. However, these nondiffracting speckles obey Rayleigh statistics, and simultaneously tailoring the speckles with non-Rayleigh statistics and nondiffraction are still unavailable now.

In this Letter, we experimentally demonstrate a method for customizing non-Rayleigh nondiffracting (NRND) speckles by encoding the wavefront of a laser beam on a spatial light modulator (SLM). Starting with the scheme of generating nondiffracting speckles, we rearrange random phases on a ring-shaped slit to generate NRND speckles, which has the specific intensity contrast $C = \sqrt{2}$ in a large longitudinal zone around the Fourier plane of the SLM. Moreover, by applying the multiple self-convolution process to the phase mask, NRND speckles with even higher contrast are also achieved. Since speckles are a valuable resource for many fundamental research and applications [38–42], we numerically simulate the Anderson localization

of light [43,44] in disordered lattices that are implemented by the NRND speckles and the results show that the localization of light can be obviously enhanced by NRND speckles with the intensity contrast higher than 1. The present work offers a method for simultaneously customizing both statistics and diffracting property of speckles, and a flexible platform to study Anderson localization.

Figure 1 shows how to design a phase mask for the generation of NRND speckles. Rayleigh statistical speckles can be generated by encoding wavefront phases that are uniformly distributed over $[-\pi, \pi]$ on a plane as shown in Fig. 1(a). The typical property of a partially coherent nondiffracting field is that all the plane-wave components are noncorrelated in the radial direction, while the correlations may be arbitrary in the azimuthal direction [31]. Thus, nondiffracting speckles can be generated by illuminating a ring-shaped slit which has a set of random phases, as shown in Fig. 1(b). However, the resulting nondiffracting speckles obey Rayleigh statistics with intensity contrast $C = 1$. For the generation of speckles with non-Rayleigh statistics, one can tailor the correlation of the scattered waves [11]. By carefully arranging random phases along the ring-shaped slit, one can introduce additional azimuthal correlations for non-Rayleigh statistics. As shown in Fig. 1(c), random phases on a ring-shaped slit are arranged with central antisymmetry $\phi(\xi, \eta) = -\phi(-\xi, -\eta)$, where (ξ, η) are the Cartesian coordinates on the phase screen and $\phi \in [-\pi, \pi]$. If such a phase mask is displayed on the front focus of a convex lens, one can obtain a speckle pattern with both non-Rayleigh statistics of enhanced intensity contrast $\sqrt{2}$ and nondiffraction on the rear focus.

The nondiffracting characteristic of the NRND speckles originates from the ring-distributed phases, and the resulting non-Rayleigh statistics can be understood with the following reason. The wavefront of the generated speckles on the rear focus is $g(x, y) \propto \iint_S d\xi d\eta e^{i\phi(\xi, \eta)} e^{-i(k/f)(x\xi + y\eta)}$, then, the intensity pattern $I(x, y)$ of the speckles on the rear focus is given by

$$I(x, y) \propto |g(x, y)|^2 \propto \left| \iint_S d\xi d\eta e^{i\phi(\xi, \eta)} e^{-i\frac{k}{f}(x\xi + y\eta)} \right|^2, \quad (1)$$

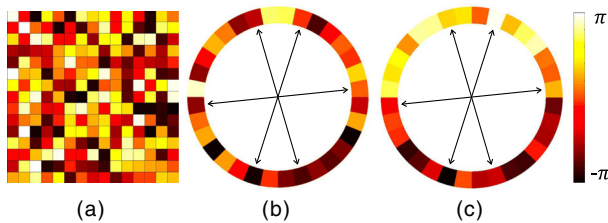


FIG. 1. Phase masks for tailoring the statistical and diffractive characteristics of speckles. (a) Random phases on a plane. (b) Random phases on a ring-shaped slit. (c) Random phases on a ring-shaped slit with central antisymmetry.

where S represents the ring-shaped area, k is the wave number of the beam, and f is the focal length of the lens. Since the intensity pattern $I(x, y)$ obeys the chi-square distribution $\chi^2(1)$, the intensity contrast [45] of $I(x, y)$ is

$$C = \frac{\sqrt{D(I)}}{\langle I \rangle} = \sqrt{2}, \quad (2)$$

where $\langle \cdot \rangle$ denotes the mean value and $D(\cdot)$ represents the variance. In this way, the non-Rayleigh statistics and nondiffracting characteristics are both introduced in the speckle pattern $I(x, y)$.

To tailor the demanded phase masks more precisely, we use the setup in the Supplemental Material [45] to generate NRND speckles. When a beam with random phases is customized right after the plane of the transparent SLM, one can obtain a standard Rayleigh statistical speckle pattern with intensity contrast $C = 1$. By applying a nonlinear transformation to the standard Rayleigh speckle and using an iterative procedure [11], a well-designed phase pattern [46] for the generation of non-Rayleigh speckle can be obtained. Figure 2(a) shows the experimentally obtained non-Rayleigh speckle with enhanced contrast of $C = 1.36$. Figure 2(b) is the experimentally recorded nondiffracting speckle pattern ($C = 0.98$) when a beam with ring-shaped and random phases comes out right after the transparent SLM. Here, the intensity profile of the nondiffracting speckle can keep stable over a range of almost 20 Rayleigh ranges. By generating a beam with antisymmetrically distributed random phases and adding a ring-shaped filtering mask on the beam, we obtain the NRND speckle as shown in Fig. 2(c). The contrast of the NRND speckle is $C = 1.35$ which is a little bit less than $\sqrt{2}$ due to the stray light introduced in the experiments.

Figures 3(a)–3(e) illustrate the nondiffracting characteristic when the NRND speckle propagates over a distance of 17 Rayleigh ranges, where the Rayleigh range in the experiment is $R = 1.85$ cm. It can be observed that the intensity profiles of these NRND speckles keep almost the same over a long distance. Figure 3(f) shows the PDFs of the nondiffracting speckles and the NRND speckles, respectively. It is clear that the nondiffracting speckles obey a negative-exponential intensity distribution. However, the PDF of the NRND speckle significantly deviates from the

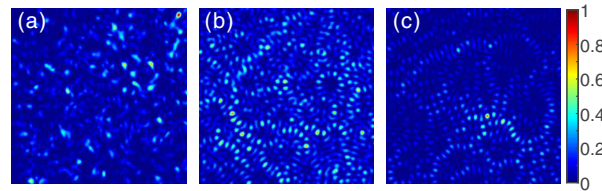


FIG. 2. Experimentally recorded speckles. (a) Non-Rayleigh speckle pattern with contrast $C = 1.36$. (b) Nondiffracting speckle pattern with $C = 0.98$. (c) NRND-speckle pattern with $C = 1.35$.

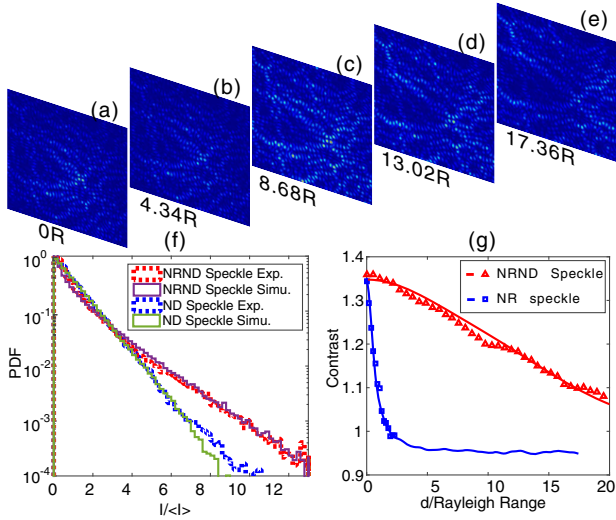


FIG. 3. Diffraction and statistical properties of NRND speckles. (a)–(e) The recorded NRND speckles at 5 axis positions: $d = 0, 4.34, 8.68, 13.02, 17.36$ Rayleigh ranges. (f) The PDFs of nondiffracting speckles and NRND speckles. Solid purple and green lines denote the computational simulated PDFs of NRND speckles and nondiffracting (ND) speckles. Dashed red and blue lines denote the experimental PDFs of NRND speckles and ND speckles. (g) The axial propagation property of contrast of non-Rayleigh speckles and NRND speckles. The triangles and squares are experimental data and solid lines are simulation results.

negative-exponential function. Moreover, the axial propagation property of the contrasts of the NRND speckles and the non-Rayleigh speckles are shown in Fig. 3(g). Here, only the data for the positive z axis are given in Fig. 3(g). As known, the statistics of the non-Rayleigh speckles changes as the beam propagates. The contrast of non-diffracting speckles in Fig. 3(g) shows a sharp drop when the observation plane is moved away from the Fourier plane of the transparent SLM, while that of NRND speckles decreases much more slowly. The full width of half maximum (FWHM) of the contrast of the non-Rayleigh speckles is about 1 Rayleigh range. When considering the data on both the negative and positive z axis, the FWHM of the contrast of the NRND speckles is about 26 Rayleigh ranges which are significantly larger than that of the non-Rayleigh speckles.

In order to generate NRND speckles with contrast higher than $C = \sqrt{2}$, it is worth studying the speckles with the wavefront of powered $g_0(x, y)$, where $g_0(x, y)$ denotes the complex amplitude of NRND speckle with contrast $C = \sqrt{2}$, because such nonlinear transformation may change the statistical property of speckles [11]. Here, we will discuss the speckle patterns with wavefront of $g_0^2(x, y), g_0^3(x, y), \dots, g_0^n(x, y), \dots$. First, it is concerned to explore the inverse Fourier transform (IFT, $\mathcal{F}^{-1}[\cdot]$) of above powered wavefront, $\mathcal{F}^{-1}[g_0^n(x, y)]$, since the phase profile of $\mathcal{F}^{-1}[g_0^n(x, y)]$ is important to the statistical and

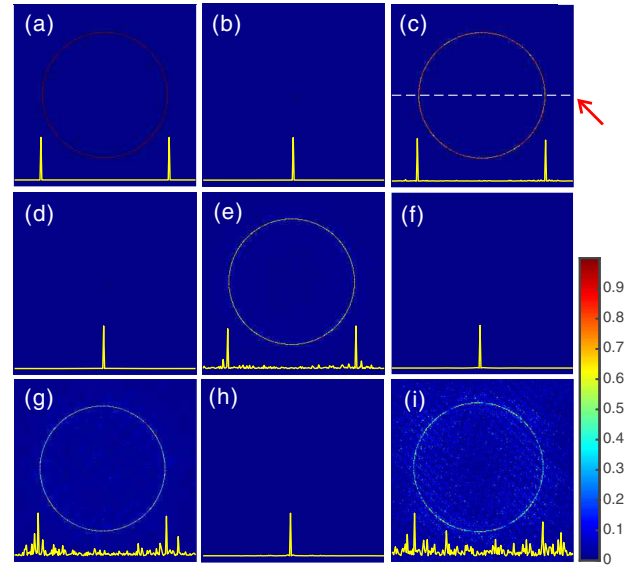


FIG. 4. The inverse Fourier transform (IFT) intensity $|\mathcal{F}^{-1}[g_0^n(x, y)]|^2$ of powered NRND-speckle pattern with complex field $g_0(x, y)$ and whose intensity contrast is $C = \sqrt{2}$. (a)–(i) are the IFT intensity patterns of complex fields $g_0(x, y), g_0^2(x, y), \dots$, and $g_0^9(x, y)$. The solid yellow line in each figure represents the detailed data of one extracted line of the IFT intensity pattern. All the extracted lines locate the same position as the white dashed line shown in (c).

diffraction characteristics of the resulting speckles. Figures 4(a)–4(i) show the numerically simulated IFT intensity $|\mathcal{F}^{-1}[g_0^n(x, y)]|^2$ of powered patterns of $g_0(x, y), g_0^2(x, y), \dots$, and $g_0^9(x, y)$, respectively. The inset yellow line in each of the figures shows the one-line data which crosses the center of the figures. It is obvious that the intensity of $|\mathcal{F}^{-1}[g_0^n(x, y)]|^2$ concentrates on a ring for the odd power, and on the center for the even power. Since the ring structure of a phase profile is the key factor for generating nondiffracting speckles, one may generate NRND speckles with higher contrast by using the phase profile of $\mathcal{F}^{-1}[g_0^n(x, y)]$ with an odd number n .

It is reasonable to assume that the information of the odd powered pattern is largely concentrated on a ring, and the information out of the ring contributes little to the demanded NRND speckles. Therefore, we can use a ring-shaped filter on the field with odd power to extract the demanded phase profiles, and this process can be used to generate NRND speckles with higher contrast than $C = \sqrt{2}$. The width of the ring will influence both the contrast and the DOF of the generated speckles. Because the wider the ring width is, the shorter the nondiffracting range is, the more information is collected from $\mathcal{F}^{-1}[g_0^n(x, y)]$, which leads to a larger contrast, and vice versa. As a result, by carefully setting the width of the ring filter to make a trade-off between the contrast and the nondiffracting range, we can generate speckles with

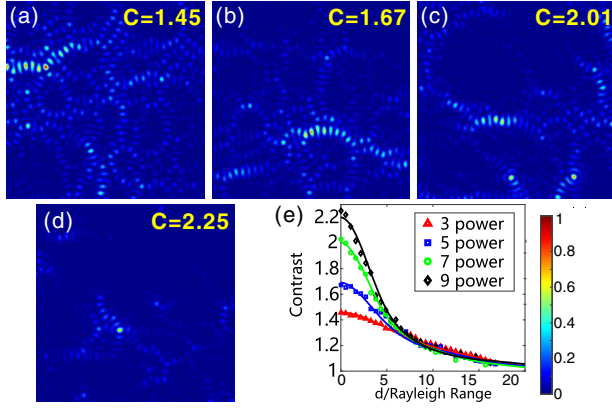


FIG. 5. Experimental generation of NRND speckles with higher intensity contrast. (a),(b),(c) and (d) Camera recorded NRND speckles with odd power $n = 3, 5, 7, 9$. (e) The axial propagation property of contrast for different odd powered NRND speckles. The dot data and solid line data represent the experimental and simulated results, respectively.

contrast higher than $C = \sqrt{2}$ and make sure that the intensity profile of the generated speckles still keeps stable over a propagation distance longer than the Rayleigh range.

In the experiments of generating NRND speckles with higher contrast, we start with one realization of NRND-speckle $g_0(x, y)$ with contrast $C = \sqrt{2}$, and calculate the IFT $\mathcal{F}^{-1}[g_0^n(x, y)]$, where n is an odd number. Then the complex amplitude of $\mathcal{F}^{-1}[g_0^n(x, y)]$ is encoded on the reflective phase SLM [45]. Next, we carefully set the transparent SLM as a ring filter to extract the demanded light pattern. Finally, the generated speckles are recorded by a charge coupled devices camera. The obtained speckles and the axial propagation property of the contrast are shown in Fig. 5. Figures 5(a)–5(d) show the observed NRND speckles with intensity contrasts $C = 1.45, 1.67, 2.01, 2.25$, respectively, when the odd powers $n = 3, 5, 7, 9$ are chosen. The axial propagation property of the contrast of these NRND speckles is shown in Fig. 5(e). It can be observed that all the FWHMs of these contrast curves are much larger than one Rayleigh range. We also demonstrate that the intensity contrast ($C > 1$) of NRND speckles can be continuously manipulated by introducing random phase noise $\alpha(\xi, \eta)$ on the input phase mask to break the antisymmetrical phase arrangement [45].

In the studies of solid-state physics, cold atoms and optical imaging, light has played a unique role for many implementations. For example, periodic and disordered photonic lattices are commonly used for the studies of localization of waves and the manipulation of atoms. Usually, the disordered photonic lattices are implemented by the superimposition of a multi-plane-waves interferometer and a speckle beam [44,47]. However, the DOF of the photonic lattices is limited by diffraction, and it is difficult to engineer the statistical property of the photonic lattices. The NRND speckle implemented in this Letter maintains

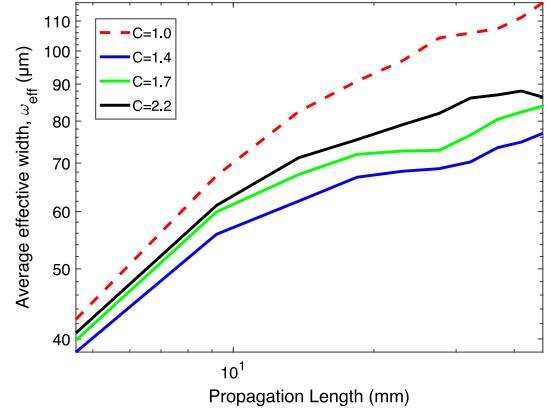


FIG. 6. The effective width ω_{eff} of the intensity profile while probe light propagating in the disordered lattice generated by speckles with various intensity contrasts. Average of over 100 realizations of NRND speckles for each kind of intensity contrast.

its random intensity profile stable over several Rayleigh ranges, behaving like a two-dimensional disordered photonic lattice and disordered waveguide array. Meanwhile, one can flexibly tailor the statistics of the photonic lattice by controlling the intensity contrast of NRND speckles.

Anderson localization of light has been investigated in various systems [44,48,49] and is important for many applications [50,51]. To illustrate the applications of the NRND speckles more clearly, we numerically simulate the Anderson localization [41,43] of light in disordered lattices which are implemented by the NRND speckles [45]. In simulations, a Gaussian beam propagates in a medium with nonuniform refractive index generated by NRND speckles with various contrast $C > 1$ and nondiffracting Rayleigh speckles with contrast $C = 1$. The probe light is always launched at the same place of the medium and over 100 realizations of NRND speckles are adopted for each kind of intensity contrast. To quantitatively demonstrate the enhancement of Anderson localization by NRND speckles, we calculated the average effective width ω_{eff} of the beam [44] while propagating through the disordered lattice generated by different nondiffracting speckles with various contrasts of $C = 1, \sqrt{2}, 1.7, 2.2$. Figure 6 presents the numerical simulated results and it shows an obvious suppression of the beam width in the disordered lattice generated by NRND speckles with intensity contrast higher than 1.

Our simulating results show that the NRND speckles with higher contrast can enhance the localization of light [45]. Thus, the NRND speckles reveal a new degree of freedom affecting the Anderson localization and offer a new platform for the exploration of the disorder statistics. Moreover, the NRND speckles may offer a flexible way for the exploration of the mobility of solitons [52,53], the dimensional crossover of cold atoms [54], and the transition from Tonks-Girardeau gas to Bosonic gas [55,56].

Based on the recent investigation of image resolution with super-Rayleigh speckle [57], the NRND speckle may also offer a possibility to achieve the enhancement of resolution and DOF of photoacoustic imaging simultaneously (see Supplemental Material for details [45]).

In summary, we propose and experimentally demonstrate a method to generate speckles which have both non-Rayleigh statistics and nondiffracting propagation simultaneously. By antisymmetrically distributing random phases on a ring-shaped slit, we can generate the NRND-speckle fields with intensity contrast $C = \sqrt{2}$. Moreover, by applying the odd-powered transformation on the NRND speckles with contrast $C = \sqrt{2}$ and introducing additional phase noises to break the central antisymmetry of the random phases, we can continuously tailor the intensity contrast of the NRND speckles. We further demonstrate the enhancement of Anderson localization of light in disordered lattices which are implemented by the NRND speckles. The resulting NRND speckles with tunable intensity statistics and nondiffracting propagation may have wide and interesting applications in the fields of the Anderson localization, optical solitons, manipulation of cold atoms, and optical imaging.

This work is supported by the National Natural Science Foundation of China (NSFC) (12074307, 92050103), Ministry of Science and Technology of the Peoples Republic of China (MOST) (2016YFA0301404), and Fundamental Research Funds for the Central Universities.

*These authors contributed equally to this work.

†shouqian.chen@hit.edu.cn

‡fli@mail.xjtu.edu.cn

- [1] J. W. Goodman, *Speckle Phenomena in Optics: Theory and Applications* (SPIE Press, Bellingham, 2020), <https://spie.org/Publications/Book/2548482?SSO=1>.
- [2] K. Kuplicki and K. W. C. Chan, High-order ghost imaging using non-rayleigh speckle sources, *Opt. Express* **24**, 26766 (2016).
- [3] L. Zhang, Y. Lu, D. Zhou, H. Zhang, L. Li, and G. Zhang, Superbunching effect of classical light with a digitally designed spatially phase-correlated wave front, *Phys. Rev. A* **99**, 063827 (2019).
- [4] L. Zhang, D. Zhou, Y. Lu, H. Zhang, and G. Zhang, Superbunched focusing with chirped random-phase gratings, *Photonics Res.* **8**, 503 (2020).
- [5] C. Ventalon and J. Mertz, Dynamic speckle illumination microscopy with translated versus randomized speckle patterns, *Opt. Express* **14**, 7198 (2006).
- [6] R. Heintzmann and M. G. Gustafsson, Subdiffraction resolution in continuous samples, *Nat. Photonics* **3**, 362 (2009).
- [7] E. Mudry, K. Belkebir, J. Girard, J. Savatier, E. Le Moal, C. Nicoletti, M. Allain, and A. Sentenac, Structured illumination microscopy using unknown speckle patterns, *Nat. Photonics* **6**, 312 (2012).
- [8] J. Gateau, T. Chaigne, O. Katz, S. Gigan, and E. Bossy, Improving visibility in photoacoustic imaging using dynamic speckle illumination, *Opt. Lett.* **38**, 5188 (2013).
- [9] N. Bender, H. Yılmaz, Y. Bromberg, and H. Cao, Introducing non-local correlations into laser speckles, *Opt. Express* **27**, 6057 (2019).
- [10] E. Jakeman and J. McWhirter, Non-gaussian scattering by a random phase screen, *Appl. Phys. B* **26**, 125 (1981).
- [11] Y. Bromberg and H. Cao, Generating non-rayleigh speckles with tailored intensity statistics, *Phys. Rev. Lett.* **112**, 213904 (2014).
- [12] J. P. Amaral, E. J. S. Fonseca, and A. J. Jesus-Silva, Tailoring speckles with weibull intensity statistics, *Phys. Rev. A* **92**, 063851 (2015).
- [13] R. Fischer, I. Vidal, D. Gilboa, R. R. B. Correia, A. C. Ribeiro-Teixeira, S. D. Prado, J. Hickman, and Y. Silberberg, Light with tunable non-markovian phase imprint, *Phys. Rev. Lett.* **115**, 073901 (2015).
- [14] X. Li, Y. Tai, H. Li, J. Wang, H. Wang, and Z. Nie, Generation of a super-rayleigh speckle field via a spatial light modulator, *Appl. Phys. B* **122**, 82 (2016).
- [15] H. E. Kondakci, A. Szameit, A. F. Abouraddy, D. N. Christodoulides, and B. E. Saleh, Sub-thermal to super-thermal light statistics from a disordered lattice via deterministic control of excitation symmetry, *Optica* **3**, 477 (2016).
- [16] Y. Zhou, F.-I. Li, B. Bai, H. Chen, J. Liu, Z. Xu, and H. Zheng, Superbunching pseudothermal light, *Phys. Rev. A* **95**, 053809 (2017).
- [17] N. Bender, H. Yılmaz, Y. Bromberg, and H. Cao, Customizing speckle intensity statistics, *Optica* **5**, 595 (2018).
- [18] N. Bender, H. Yılmaz, Y. Bromberg, and H. Cao, Creating and controlling complex light, *APL Photonics* **4**, 110806 (2019).
- [19] A. Gatti, D. Magatti, and F. Ferri, Three-dimensional coherence of light speckles: theory, *Phys. Rev. A* **78**, 063806 (2008).
- [20] D. Magatti, A. Gatti, and F. Ferri, Three-dimensional coherence of light speckles: Experiment, *Phys. Rev. A* **79**, 053831 (2009).
- [21] J. Durin, Exact solutions for nondiffracting beams. I. The scalar theory, *JOSA A* **4**, 651 (1987).
- [22] J. Durin, J. J. Miceli, and J. H. Eberly, Diffraction-Free Beams, *Phys. Rev. Lett.* **58**, 1499 (1987).
- [23] J. C. Gutiérrez-Vega, M. Iturbe-Castillo, and S. Chávez-Cerda, Alternative formulation for invariant optical fields: Mathieu beams, *Opt. Lett.* **25**, 1493 (2000).
- [24] M. A. Bandres, J. C. Gutiérrez-Vega, and S. Chávez-Cerda, Parabolic nondiffracting optical wave fields, *Opt. Lett.* **29**, 44 (2004).
- [25] G. A. Siviloglou, J. Broky, A. Dogariu, and D. N. Christodoulides, Observation of Accelerating Airy Beams, *Phys. Rev. Lett.* **99**, 213901 (2007).
- [26] J. Turunen and A. T. Friberg, Propagation-invariant optical fields, in *Progress in Optics* (Elsevier, New York, 2010), Vol. 54, pp. 1–88.
- [27] T. Vettenburg, H. I. Dalgarno, J. Nylk, C. Coll-Lladó, D. E. Ferrier, T. Čížmár, F. J. Gunn-Moore, and K. Dholakia, Light-sheet microscopy using an airy beam, *Nat. Methods* **11**, 541 (2014).

- [28] H. E. Kondakci and A. F. Abouraddy, Diffraction-free pulsed optical beams via space-time correlations, *Opt. Express* **24**, 28659 (2016).
- [29] M. Yessenov and A. F. Abouraddy, Accelerating and Decelerating Space-Time Optical Wave Packets in Free Space, *Phys. Rev. Lett.* **125**, 233901 (2020).
- [30] J. Baumgartl, M. Mazilu, and K. Dholakia, Optically mediated particle clearing using airy wavepackets, *Nat. Photonics* **2**, 675 (2008).
- [31] J. Turunen, A. Vasara, and A. T. Friberg, Propagation invariance and self-imaging in variable-coherence optics, *JOSA A* **8**, 282 (1991).
- [32] D. M. Cottrell, J. M. Craven, and J. A. Davis, Nondiffracting random intensity patterns, *Opt. Lett.* **32**, 298 (2007).
- [33] C. López-Mariscal and K. Helmersson, Shaped nondiffracting beams, *Opt. Lett.* **35**, 1215 (2010).
- [34] A. Dudley, R. Vasilyeu, V. Belyi, N. Khilo, P. Ropot, and A. Forbes, Controlling the evolution of nondiffracting speckle by complex amplitude modulation on a phase-only spatial light modulator, *Opt. Commun.* **285**, 5 (2012).
- [35] S. G. Reddy, P. Chithrabhanu, P. Vaity, A. Aadhi, S. Prabhakar, and R. Singh, Non-diffracting speckles of a perfect vortex beam, *J. Optics* **18**, 055602 (2016).
- [36] R. Chriki, G. Barach, C. Tradosny, S. Smartsev, V. Pal, A. A. Friesem, and N. Davidson, Rapid and efficient formation of propagation invariant shaped laser beams, *Opt. Express* **26**, 4431 (2018).
- [37] D. Phillips, R. He, Q. Chen, G. Gibson, and M. Padgett, Non-diffractive computational ghost imaging, *Opt. Express* **24**, 14172 (2016).
- [38] F. Scheffold and G. Maret, Universal Conductance Fluctuations of Light, *Phys. Rev. Lett.* **81**, 5800 (1998).
- [39] J. Billy, V. Josse, Z. Zuo, A. Bernard, B. Hambrecht, P. Lugan, D. Clément, L. Sanchez-Palencia, P. Bouyer, and A. Aspect, Direct observation of anderson localization of matter waves in a controlled disorder, *Nature (London)* **453**, 891 (2008).
- [40] J. Wang and A. Z. Genack, Transport through modes in random media, *Nature (London)* **471**, 345 (2011).
- [41] M. Segev, Y. Silberberg, and D. N. Christodoulides, Anderson localization of light, *Nat. Photonics* **7**, 197 (2013).
- [42] B. Redding, S. F. Liew, R. Sarma, and H. Cao, Compact spectrometer based on a disordered photonic chip, *Nat. Photonics* **7**, 746 (2013).
- [43] P. W. Anderson, Absence of diffusion in certain random lattices, *Phys. Rev.* **109**, 1492 (1958).
- [44] T. Schwartz, G. Bartal, S. Fishman, and M. Segev, Transport and anderson localization in disordered two-dimensional photonic lattices, *Nature (London)* **446**, 52 (2007).
- [45] See Supplemental Material <http://link.aps.org/supplemental/10.1103/PhysRevLett.127.180601> for a detailed description of the theoretical analyses of intensity contrast of speckles, experimental setup, continuously tailoring the intensity contrast of NRND speckles, numerical simulation of the enhanced Anderson localization of light and the discussion of possible applications of NRND speckles.
- [46] E. Bolduc, N. Bent, E. Santamato, E. Karimi, and R. W. Boyd, Exact solution to simultaneous intensity and phase encryption with a single phase-only hologram, *Opt. Lett.* **38**, 3546 (2013).
- [47] N. K. Efremidis, S. Sears, D. N. Christodoulides, J. W. Fleischer, and M. Segev, Discrete solitons in photorefractive optically induced photonic lattices, *Phys. Rev. E* **66**, 046602 (2002).
- [48] H. H. Sheinfux, Y. Lumer, G. Ankonina, A. Z. Genack, G. Bartal, and M. Segev, Observation of anderson localization in disordered nanophotonic structures, *Science* **356**, 953 (2017).
- [49] J.-C. Garreau, Quantum simulation of disordered systems with cold atoms, *C. R. Phys.* **18**, 31 (2017).
- [50] H. Cao, J. Y. Xu, D. Z. Zhang, S.-H. Chang, S. T. Ho, E. W. Seelig, X. Liu, and R. P. H. Chang, Spatial Confinement of Laser Light in Active Random Media, *Phys. Rev. Lett.* **84**, 5584 (2000).
- [51] V. A. Podolskiy, E. Narimanov, W. Fang, and H. Cao, Chaotic microlasers based on dynamical localization, *Proc. Natl. Acad. Sci. U.S.A.* **101**, 10498 (2004).
- [52] N. K. Efremidis and K. Hizanidis, Disordered Lattice Solitons, *Phys. Rev. Lett.* **101**, 143903 (2008).
- [53] Y. V. Kartashov, B. A. Malomed, and L. Torner, Solitons in nonlinear lattices, *Rev. Mod. Phys.* **83**, 247 (2011).
- [54] H. Zhai, *Ultracold Atomic Physics* (Cambridge University Press, Cambridge, England, 2021).
- [55] B. Paredes, A. Widera, V. Murg, O. Mandel, S. Fölling, I. Cirac, G. V. Shlyapnikov, T. W. Hänsch, and I. Bloch, Tonks–girardeau gas of ultracold atoms in an optical lattice, *Nature (London)* **429**, 277 (2004).
- [56] J. Radić, V. Bačić, D. Jukić, M. Segev, and H. Buljan, Anderson localization of a tonks-girardeau gas in potentials with controlled disorder, *Phys. Rev. A* **81**, 063639 (2010).
- [57] P. Liu, Label-free storm principle realized by super-rayleigh speckle in photoacoustic imaging, *Opt. Lett.* **44**, 4642 (2019).